

Guided magnonic Michelson interferometer

Muhammad H. Ahmed,¹ Jan Jeske,¹ and Andrew D. Greentree^{1,2}

¹*Chemical and Quantum Physics, School of Applied Sciences, RMIT University, Melbourne 3001, Australia*

²*ARC Centre of Excellence in Nanoscale BioPhotonics,
School of Applied Sciences, RMIT University, Melbourne, VIC 3001, Australia*
(Dated: November 4, 2022)

Magnonics is an emerging field with potential applications in classical and quantum information processing. Freely propagating magnons in two-dimensional media suffer from dispersion, which limits their effective range and fidelity. We show the design of controllable magnonic circuitry, that utilise surface current carrying wires to create magnonic waveguides. We also show the design of a magnonic directional coupler and controllable Michelson interferometer to demonstrate its utility for information processing tasks.

PACS numbers: 75.10.Pq, 03.67.Hk, 05.60.Gg, 75.30.Ds

I. INTRODUCTION

During the past two decades, magnonics has become a major field of theoretical and experimental research¹⁻³. The potential use of spin waves in several technologies, like computing (quantum⁴ and classical⁵⁻⁷), communication⁸ and caloritronics⁹ has been investigated thoroughly. Magnon-magnon scattering also provides an interesting test bed for exploring more general particle-particle interactions^{10,11}. The core idea of magnonics is to manipulate spin waves in ferromagnetic or anti-ferromagnetic materials, and in doing so to produce devices with different functionalities^{2,5,12}. This manipulation is usually achieved by the application of the external fields¹³⁻¹⁵, by crafting the material itself^{16,17} or some combination of both^{12,18}. In a magnonic device there is no net transport of charge as opposed to electronic devices, where current flow leads to inevitable heating. For this reason, magnonic technology promises the advantage of reduced power consumption compared to its electronic counterparts.

A spin wave is a propagating disturbance in an otherwise perfectly ordered magnetic media^{19,20}. When quantised, the associated particle is a magnon. Here we are concerned with the propagation of magnons confined to a two dimensional array of spin-1/2 particles (spin sheet). Within the sheet, each spin interacts with its nearest neighbour through exchange or dipole-dipole coupling. Due to this interaction they either align (ferromagnetic coupling) or anti-align (anti-ferromagnetic coupling) themselves to their nearest neighbours, resulting in a global order in spin direction as the lowest energy state. Any disturbance in the global order creates propagating magnons in the sheet¹.

Freely propagating magnons are subject to damping and dispersion, which limits the distances over which the magnon can propagate²¹. The effects of dispersion can be mitigated by confining the magnon in the direction transverse to the travel direction. Typically, such confinement is achieved by lithographically removing material to leave a magnonic channel^{22,23}, that minimise the transversal

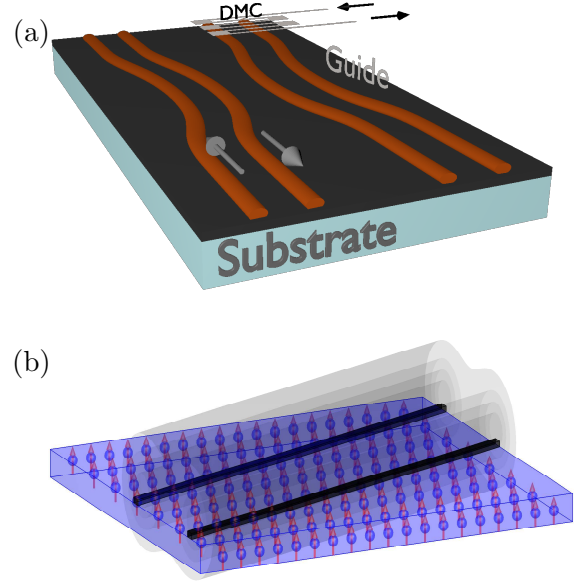


FIG. 1. (a) Schematic of the Magnonic Michelson interferometer. Black layer shows two-dimensional ferromagnetic sheet on a substrate. Brown lines are current carrying wires and the arrows show the direction of current in wires. One arm has a dynamic magnonic crystal (DMC) at its end for the purpose of phase addition. (b) Schematic of spin guide. Black lines represent current carrying wire. Black translucent surfaces are magnitude field contours.

dispersion. However, such approaches are not suited to reconfigurable devices due to the permanent structural changes induced in the material.

Here we describe a method of confining and transporting a magnon in a two-dimensional ferromagnetic film, which does not require any structural modification of the film itself. In our model, the confinement is achieved by the magnetic field from two parallel current-carrying wires placed on the surface at some distance from each other. When the current direction in the wires is opposite, the resultant magnetic field forms a potential well,

creating a channel for the magnons. Previously we have shown analogous confinement in one-dimensional spin chains using a surface-gate array, where the transport was achieved through the adiabatic temporal variation of the potential^{24,25}.

Our results enable reconfigurable magnonic circuitry of several potentially interacting magnon channels that preserve magnon phase and thereby enable quantum information processing. The channels can be reconfigured by adapting the current in the wires that create the channel. One can consider multiple spin-guides on a single surface and can switch them on or off as desired. This ability can be used to build complex magnonic circuitry for all-magnon information processing.

More generally, our work is motivated by efforts to demonstrate traditional quantum optical effects in non-traditional tight-binding systems^{25–28}.

To illustrate the utility of our scheme, we present a full design for a guided magnon version of a Michelson interferometer. The Michelson interferometer is an important element for high-precision sensing and can also be used as a primitive for switching in all-magnon logic gates³⁰.

This paper is set out as follows. We first introduce the Heisenberg Hamiltonian in two dimensions and a magnon confining potential. We then consider the extension to a directional coupler and finally a magnonic Michelson Interferometer.

II. FREE AND GUIDED MAGNON PROPAGATION IN A 2D FILM

To calculate the magnon propagation, we introduce the Heisenberg Hamiltonian with nearest neighbour interaction in two dimensional square lattice.

$$H = -J \sum_{i,j} \vec{\sigma}_{i,j} \cdot \vec{\sigma}_{i+1,j} + \vec{\sigma}_{i,j} \cdot \vec{\sigma}_{i,j+1} + B_{i,j} \sigma_{i,j}^z, \quad (1)$$

where i and j are the spin indices along each spin-sheet dimension, $\vec{\sigma}_{i,j} = (\sigma_{i,j}^x, \sigma_{i,j}^y, \sigma_{i,j}^z)$ and $\sigma_x, \sigma_y, \sigma_z$ are the Pauli spin matrices. J is the strength of nearest neighbour interaction, which without loss of generality we take as the exchange interaction.

The second term in the Hamiltonian is the on-site energy of the (i, j) th spin due to the local external magnetic field $B_{i,j}$. The dispersion relation of a freely propagating magnon in a two dimensional sheet is

$$\omega_{k_x, k_y} = 4J - 2J[\cos(k_x a) + \cos(k_y a)], \quad (2)$$

where ω is the angular frequency of a particular eigenmode, k_x and k_y are the wave number along x and y directions and a is the spin spacing. To illustrate the free magnon dispersion we considered a magnon with the initial wave function

$$\psi(x_i, y_j) = \exp \left[-\frac{(x_0 - x_i)^2}{2\sigma_x^2} - \frac{(y_0 - y_j)^2}{2\sigma_y^2} \right] \exp^{-ik_x x - ik_y y} \quad (3)$$

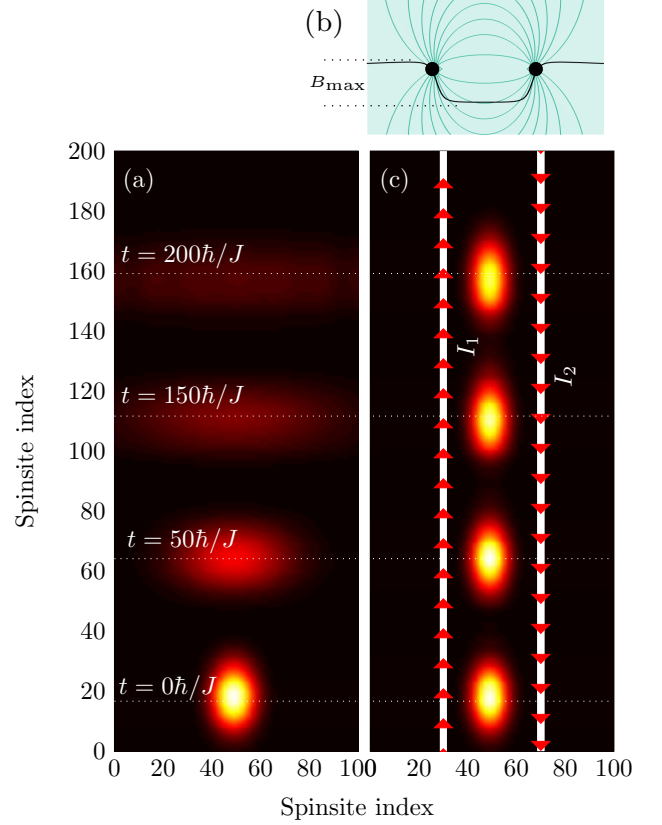


FIG. 2. (a) Snap shots showing a free magnon propagating on a spin-sheet for different times. The magnon shows large dispersion in the transversal direction as it propagates. (b) Contour lines of combined absolute magnetic field of two wires, taken perpendicular to the direction of wires. Black dots show the position of wires, where the black line is the net z-component as seen by the spins, which are located 10nm below the wires. (c) Magnon confined by the surface current carrying wires for same initial state as (a). The red arrows show the direction of the current. These wires were placed 40 spin sites apart and the depth of the potential is $B_{\max} = 2[J/\gamma\hbar]$. After the confinement there is no transverse spreading of magnon.

This corresponds to a Gaussian wavepacket propagating in the x and y -direction with the initial group velocity corresponding to wave vector k_x and k_y . σ_x and σ_y are the standard deviations in x and y -directions and (x_0, y_0) is the center of the wave packet. The required k -vector to achieve a certain group velocity of the magnon can be calculated by the following relation

$$v_g = \frac{\partial \omega}{\partial k} = \frac{2Ja}{\hbar} \sin(ka). \quad (4)$$

In our simulation we initiated the magnon with a y-velocity of 2 sites per unit time (\hbar/J), which corresponds to $k_y a = \pi/2$ and $k_x = 0$.

Figure 2(a) shows the evolution of the wave packet along the spin sheet. We observe asymmetric dispersion in the respective directions. In the propagation direction,

the group velocity is closer to the linear part of the dispersion relation of the dispersion curve, hence it shows reduced dispersion.

For our confinement scheme, two current carrying wires with anti-parallel current produce a magnetic field as shown in Fig. 2(b). Superimposed on this is the confining potential (black line) as seen by the magnons. In addition to the field of the wires we also applied a global z-field which is large compared wires magnetic field. This large field energetically separates the total ground state from the single-excitation subspace, and also allows the secular approximation. The secular approximation allows us to neglect all terms from non-z components of the wire-field because they are averaged out by the strong z-field. Hence we perform all calculations in the single excitation subspace and ignore the x and y magnetic field components due to the wires. To get the effective Oersted field we performed a complete numerical integration over the length of the wire. For the rest of the paper we express the magnetic field (B), which determine the on-site energies of spin in Hamiltonian, in the reduced units of $J/\gamma\hbar$, where J is the coupling strength and γ is the gyromagnetic ratio of the electron.

Figure 2(c) shows the evolution of a magnon in the guide. As expected, there is negligible transverse dispersion, however the longitudinal dispersion is unchanged. The white lines show the wires and the red arrows show the direction of current in the wires.

Our spin guide model provides confinement analogous to that in optical wave guides and it can show similar functionalities, for example, bending and coupling. Although, the shape will have an effect on the properties like adiabatic bending and coupling, which we discuss in detail in the next section. The exact shape of the confining potential is not important, as long as the potential is strong enough to create one or more confined modes.

Turning our attention to bend loss, in Fig. 3 we show three different bending regimes. When the radius of curvature of the bend is large, the magnon can follow the guide adiabatically [Fig. 3(a)]. As the radius of curvature reduces, the magnon will excite higher modes, although, here it still stays confined to the guide [Fig. 3(b)]. In this kind of bending, the quantum phase is not preserved, so it is not a useful regime for quantum transport. And finally, when the bend becomes very sharp (small radius of curvature), the magnon can not follow the guide anymore and it leaks out into unconfined modes [Fig. 3(c)].

III. MAGNON SPLITTER, AND THE MICHELSON INTERFEROMETER

We now address the issue of the design of a magnonic Michelson interferometer. The Michelson interferometer comprises an input channel, a splitter element (beam-splitter or directional coupler), a variable (ideally tunable) phase element, and a reflective element that directs the signal back to the splitter. The final output path

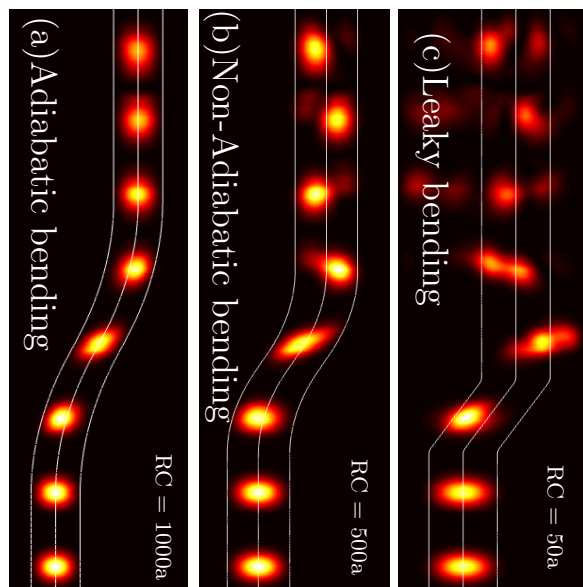


FIG. 3. Effect of the guide bending on the quality of transport. Each subfigure is an overlaid snapshots of equally spaced time evolved states, where RC is the radius of curvature of the bend. (a) Adiabatic bending, in which the magnon stays in the transversal ground state through out the propagation. (b) As we make the bend tighter, the magnon starts to excite higher modes, although, it still stays confined in the guide. (c) At small bend radius the magnon completely leaks out.

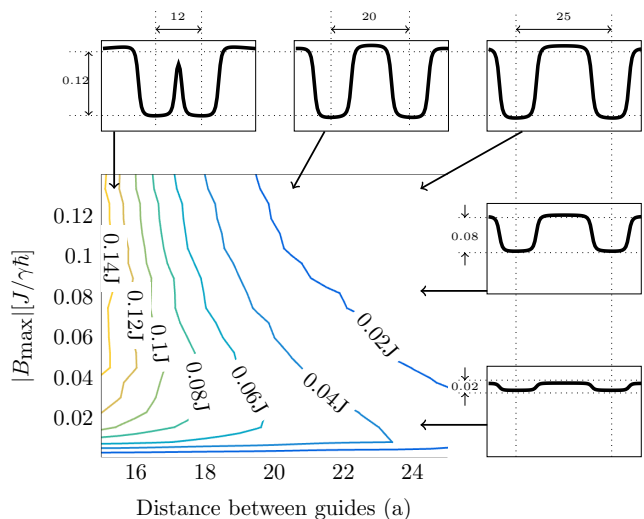


FIG. 4. Contours of constant coupling of two directionally coupled spin guides, as a function of the depth of the potential and the separation between them. The coupling strength decreases with increasing depth as well as with increasing separation between guides. At small currents, the modes become unbound. The thumbnails on the top and right sides show cross sections of the magnetic field perpendicular to the guiding direction, to illustrate the relative change in the shape of the potential along both axes.

of the magnon then becomes a sensitive function of the variable phase. We discuss these elements in turn.

The directional coupler is an important and commonly used device in optical fiber technology. Typically a directional coupler requires two proximal guides so that particles evanescently hop from one guide to the other. Similarly, we can achieve the same functionality with our magnonic analogs. When two guides are close to each other, the magnon can coherently tunnel between the guides and this tunnelling rate varies as a function of both the distance between the guides and the depth of the guides. If the guides are made lithographically, then the separation between the guides cannot be varied post fabrication, however the depth of the guides can be easily modified using the magnitude of the current. Hence we can realise reconfigurable directional couplers. Figure 4 shows contours of constant coupling energy as a function of current and guide separation using the same geometries used previously. The coupling is stronger when the guides are closer and shallower (small current). The coupling reduces with the increase in distance and the increase in current.

The Michelson interferometer requires the guides to be isolated from each other before and after the directional coupler. Defining $|L\rangle$ and $|R\rangle$ as the basis states of the interferometer, where $|L\rangle$ is the magnon in the left arm and $|R\rangle$ is the magnon in the right arm and with out the loss of generality we always start the magnon in state $|L\rangle$. We envisage adiabatically reducing the distance between the guides to effect the directional coupler, and then adiabatically increasing the distance after half of the population has been transferred, i.e. we have performed the transformation $|L\rangle \rightarrow (1/\sqrt{2})(|L\rangle + |R\rangle)$. We achieved this with a set of simulations, where we started the guides at 35 sites apart and then adiabatically reduced the distance between them to 23 sites, where the width of each guide is 20 sites and the radius of the curvature of bend was 5000 sites. They stay coupled at this distance for 650 sites, before turning away from each other, as shown in Fig. 5(a). We used current of 0.5mA, which resulted in B_{max} of $2[J/\gamma\hbar]$.

There are many ways in which a controllable phase shift can be introduced. Here we modelled a dynamic magnonic crystal-like structure¹⁴ at the end of one arm, as shown in Fig. 5(b), which acts as a tuneable phase source. A dynamic magnonic crystal is an array of equidistant conducting wires placed on the top of magnetic media. The flow of current in these wires causes a periodic magnetic perturbation in the magnetic film as shown in Fig. 5 (c). The depth of the perturbation can be controlled by controlling the current in the wires³¹. In our case the periodicity of the magnonic crystal was chosen to be 10 spin sites with 20 periods. As we change the current in the crystal, it changes the amount of extra phase that has been added to the right arm magnon path.

Finally we realise the reflection by the hard wall boundary condition at the edge of the spin sheet, which

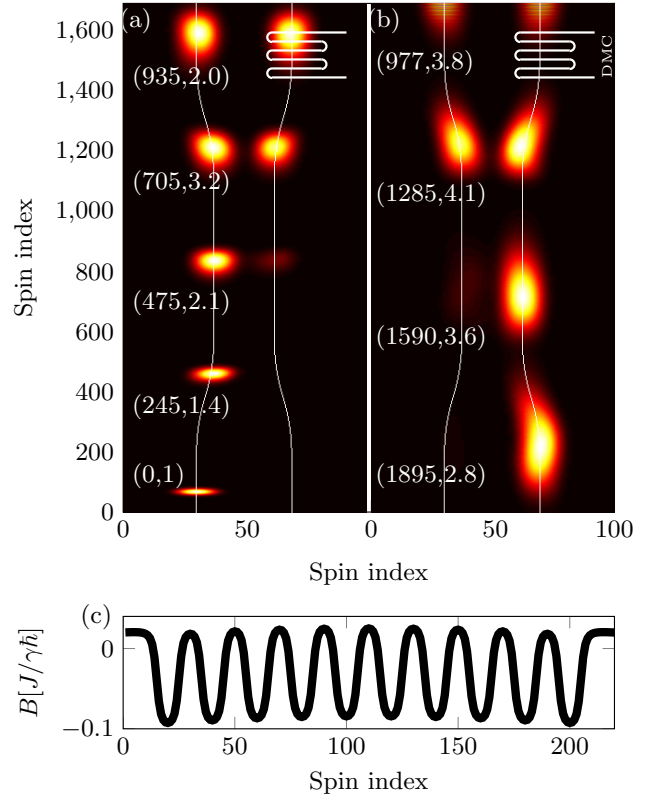


FIG. 5. An instance of full time evolution of a Michelson interferometer. White lines represent the centre of each guide. Snap shots of the population are overlaid on top of each other. Each snapshot is scaled such that it appears equally bright as the first snapshot. Numbers placed next to each snap shot are time stamp (in units of \hbar/J) and scaling factor respectively. (a) The magnon was initialised in state $|L\rangle$ and it splits into $(1/\sqrt{2})(|L\rangle + |R\rangle)$ upon passing through the splitter. In this particular instance there is no relative phase shift upon reflection. (b) After reflection and second pass through the splitter the magnon is transmitted to $|R\rangle$. (c) The magnetic field cross section of the magnetic field of the DMC ($I = 1\text{mA}$) inside the spin sheet.

reverses the direction of the magnon but does not introduce any relative phase between the two arms of the interferometer. After reflection, the right arm passes the dynamic magnon crystal a second time, doubling the effect of its phase shift.

The final state of the interferometer is only a function of the relative phase between the arms, which in turn is a function of current in the crystal. Fig. 5 shows the evolution where no extra phase ($\phi = 0$) is added to the magnon. Figure 5(a) shows the propagation up to the reflection, whereas Fig. 5(b) shows the propagation after the reflection. The double passing of the beamsplitter has resulted in the magnon being shifted from $|L\rangle$ to $|R\rangle$.

Increasing the current in the crystal leads to a relative phase shift seen in the right arm (Fig. 6). This leads to a sinusoidal variation in the final population in each arm as a function of the phase shift, as is ex-

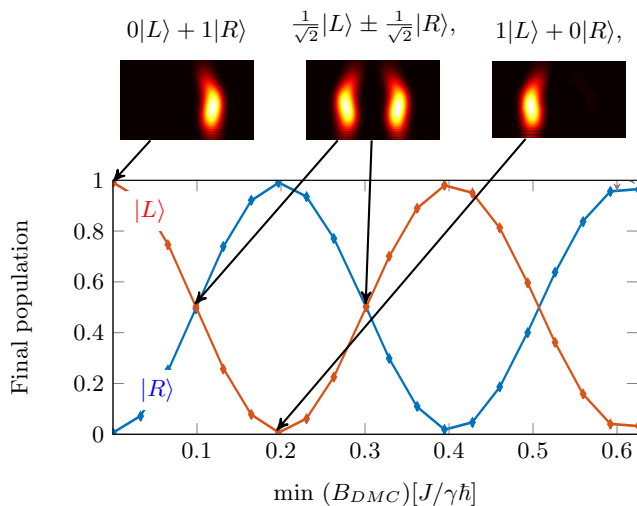


FIG. 6. Population in each arm at the end of the protocol, as a function of the depth of the potential due to the magnonic crystal, which in turn is the function of current in the crystal. Red is the population in left arm and blue is the population in right arm. As the potential depth increases, population in each arm starts to vary sinusoidally between zero and one in sinusoidal fashion. It goes through the whole state space and come back to the original state at $\min(B_{DMC}) = 0.4[J/\gamma\hbar]$.

pected. When $\min(B_{DMC}) = -0.1[J/\gamma\hbar]$ the final population is equal in each arm $(1/\sqrt{2})(|L\rangle + |R\rangle)$, where $\min(B_{DMC})$ is the maximum depth of the magnonic crystal field. As we keep increasing the current, the trend continues and the final state goes through $|R\rangle$, $(1/\sqrt{2})(|L\rangle - |R\rangle)$ and eventually coming back to $|L\rangle$ at $\min(B_{DMC}) = 0.4[J/\gamma\hbar]$. This shows that the current through the dynamic magnon crystal can be used as a tunable element for magnon switching.

IV. CONCLUSION

We have proposed a novel scheme for guiding magnons in a two-dimensional ferromagnetic sheet using surface current carrying wires. Through numerical simulation based on the Heisenberg model, we demonstrated that transversal confinement can be achieved in this setup. We also presented a model of a magnonic Michelson interferometer. The magnon is split and recombined using a magnonic equivalent of a directional coupler. The extra phase was added onto one arm through a dynamical magnonic crystal. By changing the amount of current in the crystal one can obtain any desired combination of population in each arm. Equally, this device could be used as a sensor of any system capable of potentially perturbing the acquired magnon phase.

One possibility afforded by our scheme is the design of magnonic devices capable of performing non-deterministic linear magnonic quantum computation, by analogy with non-deterministic linear optical quantum computation³². Non-deterministic linear schemes utilise interferometric elements and the ‘hidden’ nonlinearity introduced by measurement. When magnons are distributed over many spins, as we have considered here, then they behave as simple type II bosons, and therefore show bunching in Hong-Ou-Mandel type configurations³³. Therefore our results imply that full non-deterministic quantum gate operations can be simply ported to the magnonic case. One further advantage of our reconfigurable scheme is that it is possible to dynamically switch guides on and off, and this may lead a natural realisation of schemes with ‘shortcuts’ through high dimensional spaces³⁴, and more generally to non-trivial consideration of optimisation of the Hilbert-space dimensionality of the resulting magnonic circuit for optimal computation³⁵.

ACKNOWLEDGMENTS

The authors would like to thank Jared Cole and Ivan Maksymov, for useful discussions. This work was supported by the Australian Research Council (Grant No. DP130104381).

- ¹ V. V. Kruglyak, S. O. Demokritov, and D. Grundler, Journal of Physics D: Applied Physics **43**, 264001 (2010).
- ² B. Lenk, H. Ulrichs, F. Garbs, and M. Münzenberg, Physics Reports **507**, 107 (2011).
- ³ A. V. Chumak, V. I. Vasyuchka, A. A. Serga, and B. Hillebrands, Nature Physics **11**, 453 (2015).
- ⁴ A. Khitun, R. Ostroumov, and K. L. Wang, Physical Review A **64**, 062304 (2001).
- ⁵ A. V. Chumak, A. A. Serga, and B. Hillebrands, Nature Communications **5**, 4700 (2014).
- ⁶ A. Khitun, M. Bao, and K. L. Wang, IEEE Transactions on Magnetics **44**, 2141.

- ⁷ A. Khitun, M. Bao, and K. L. Wang, Journal of Physics D: Applied Physics **43**, 264005 (2010).
- ⁸ K. Vogt, F. Y. Fradin, J. E. Pearson, T. Sebastian, S. D. Bader, B. Hillebrands, A. Hoffmann, and H. Schultheiss, Nature Communications **5** (2014).
- ⁹ G. E. W. Bauer, E. Saitoh, and B. J. van Wees, Nature Materials **11**, 391 (2012).
- ¹⁰ S. Bose, Contemporary Physics **48**, 13 (2007).
- ¹¹ P. Longo, A. D. Greentree, K. Busch, and J. H. Cole, Physics Letters A **377**, 1242 (2013).
- ¹² T. Schneider, A. A. Serga, B. Leven, B. Hillebrands, R. L. Stamps, and M. P. Kostylev, Applied Physics Letters **92**,

- 022505 (2008).
- ¹³ A. A. Serga, T. Neumann, A. V. Chumak, and B. Hillebrands, *Applied Physics Letters* **94**, 112501 (2009).
 - ¹⁴ A. V. Chumak, T. Neumann, A. A. Serga, B. Hillebrands, and M. P. Kostylev, *Journal of Physics D: Applied Physics* **42**, 205005 (2009).
 - ¹⁵ T. Neumann, A. A. Serga, and B. Hillebrands, *Applied Physics Letters* **94**, 042503 (2009).
 - ¹⁶ A. V. Chumak, A. A. Serga, S. Wolff, B. Hillebrands, and M. P. Kostylev, *Applied Physics Letters* **94**, 172511 (2009).
 - ¹⁷ Y. V. Gulyaev, S. A. Nikitov, L. V. Zhivotovskii, A. A. Klimov, P. Tailhades, L. Presmanes, C. Bonningue, C. S. Tsai, S. L. Vysotskii, and Y. A. Filimonov, *Jetp Letters* **77**, 567 (2003).
 - ¹⁸ M. P. Kostylev, A. A. Serga, T. Schneider, B. Leven, and B. Hillebrands, *Applied Physics Letters* **87**, 153501 (2005).
 - ¹⁹ F. J. Dyson, *Phys.Rev.* **102**, 1217 (1956).
 - ²⁰ W. Heisenberg, *Zeitschrift für Physik* **49**, 619 (1928).
 - ²¹ A. A. Serga, A. V. Chumak, and B. Hillebrands, *Journal of Physics D: Applied Physics* **43**, 264002 (2010).
 - ²² A. V. Chumak, P. Pirro, A. A. Serga, M. P. Kostylev, R. L. Stamps, H. Schultheiss, K. Vogt, S. J. Hermsdoerfer, B. Laegel, P. A. Beck, and B. Hillebrands, *Applied Physics Letters* **95**, 262508 (2009).
 - ²³ S. V. Vasiliev, V. V. Kruglyak, M. L. Sokolovskii, and A. N. Kuchko, *Journal of Applied Physics* **101**, 113919 (2007).
 - ²⁴ M. I. Makin, J. H. Cole, C. D. Hill, and A. D. Greentree, *Physical Review Letters* **108**, 017207 (2012).
 - ²⁵ M. H. Ahmed and A. D. Greentree, *Physical Review A* **91**, 022306 (2015).
 - ²⁶ G. M. Nikolopoulos, *Physical Review Letters* **101**, 200502 (2008).
 - ²⁷ M.-H. Yung and S. Bose, *Physical Review A* **71**, 032310 (2005).
 - ²⁸ M. I. Makin, J. H. Cole, C. D. Hill, A. D. Greentree, and L. C. L. Hollenberg, *Physical Review A* **80**, 043842 (2009).
 - ²⁹ A. L. C. Hayward, A. M. Martin, and A. D. Greentree, *Physical Review Letters* **108**, 223602 (2012).
 - ³⁰ S. Klingler, P. Pirro, T. Brächer, B. Leven, B. Hillebrands, and A. V. Chumak, *Applied Physics Letters* **105**, 152410 (2014).
 - ³¹ M. Krawczyk and D. Grundler, *J. Phys.: Condens. Matter* **26**, 123202 (2014).
 - ³² E. Knill, R. Laflamme, and G. J. Milburn, *Nature* **409**, 46 (2001).
 - ³³ C. K. Hong, Z. Y. Ou, and L. Mandel, *Physical Review Letters* **59**, 2044 (1987).
 - ³⁴ B. P. Lanyon, M. Barbieri, M. P. Almeida, T. Jennewein, T. C. Ralph, K. J. Resch, G. J. Pryde, J. L. O'Brien, A. Gilchrist, and A. G. White, *Nature Physics* , 134 (2008), 0804.0272.
 - ³⁵ A. D. Greentree, S. G. Schirmer, F. Green, L. C. L. Hollenberg, A. R. Hamilton, and R. G. Clark, *Physical Review Letters* **92**, 097901 (2004).